Al-Nahrain Journal for Engineering Sciences **NJES** 27(3)336-345, 2024
http://doi.org/10.29194/NJES.27030336

Microstructure and Compressive Peak Stress Analyses of 3D Printed TPU MM-3520

Ahmed A. Ameen[1*], Ayad M. Takhakh[2], Abdalla Abdal-hay[3, 4, 5]

Authors affiliations:
1*) Mechanical Engineering Department, College of Engineering Department, Al-Nahrain University, Baghdad 10072, Iraq.
ahmeda.ameen94@gmail.com
2) Mechanical Engineering Department, College of Engineering Department, Al-Nahrain University, Baghdad 10072, Iraq.
ayadmurad@nahrainuniv.edu.iq
3) Faculty of Industry and Energy Technology, Mechatronics Technology Program, New Cairo Technological University, New Cairo - Fifth Settlement, Cairo 11835, Egypt.
4) Department of Engineering Materials and Mechanical Design, Faculty of Engineering, South Valley University, Qena 83523, Egypt.
5) The University of Queensland, School of Dentistry, Oral Health Centre Herston, 288 Herston Road, Herston, QLD 4006, Australia.
abdalla.ali@uq.edu.au

Paper History:

Received: 7th May 2024

Revised: 13th Sep. 2024

Accepted: 4th Oct. 2024

Abstract

Specimens with the structure of a face-centered cubic were produced using several sets of printing conditions. An experimental testing is conducted to carefully evaluate the microstructural analysis and compressive strength of this structure. The results include the measurement of mechanical properties, such as the peak stress. Fused deposition modeling is employed for the additive manufacturing of experimental specimens made from shape memory polymer thermoplastic polyurethane (MM-3520). We take into account the impact of printing factors on lattice structures, such as layer thickness, printing temperature, and printing speed. Analyzing the microstructure of the printed specimens exhibits that the specimens with highest printing temperature, lowest printing speed and thinner printing layer have better layers adhesion and lower porosities. All the mechanical tests are performed on specimens with the same structure and at a relatively constant density. Among the tested printing parameters, using a layer height of 0.1 mm, a printing temperature of 230 °C, and a printing speed of 20 mm/s yields the highest strength in the specimens. However, specimens printed with a layer height of 0.2 mm, a printing temperature of 220 °C, and a printing speed of 30 mm/s also exhibit good strength, albeit slightly lower than the maximum values. Additionally, when using these specific settings (0.3 mm – 210 °C – 40 mm/s), the mechanical qualities are minimized, yet the stress-strain curves exhibit characteristics similar to elastomers.

Keywords: Fused Deposition Modeling, Shape Memory Polymer, Printing Parameters, Mechanical Properties.

تحليل البنية المجهرية و ذروة اجهاد الضغط لـTPU MM-3520 المطبوع بطريقة ثلاثي الابعاد

أحمد عباس أمين ، أياد مراد طخاخ، عبد الله عبد الحي

الخلاصة:

تم إنتاج عينات ذات بنية مكعبة محورها الوجه باستخدام عدة مجاميع من محددات الطباعة. حيث أُجريت اختبارات عملية لتقييم التحليل المجهري وقوة الضغط لهذا الهيكل بعناية. وتشمل النتائج قياس الخواص الميكانيكية، مثل ذروة الإجهاد. تم استخدام طرية التشكيل بترسيب المنصهر في التصنيع بالاضافة للعينات التجريبية المصنوعة من بوليمر البولي يوريثين الحراري ذو الذاكرة الشكلية (MM-3520). و أخذنا في الاعتبار تأثير عوامل الطباعة على الهياكل الشبكية، مثل سمك الطبقة، ودرجة حرارة الطباعة، وسرعة الطباعة. يُظهر تحليل البنية المجهرية للعينات المطبوعة أن العينات ذات أعلى درجة حرارة للطباعة وأقل سرعة طباعة وطبقة طباعة أرق تتمتع بطبقات التصاق أفضل ومسامية أقل. كما تم إجراء جميع الاختبارات الميكانيكية على عينات لها نفس البنية وبكثافة ثابتة نسبيًا. من بين معلمات الطباعة التي تم اختبارها، فإن استخدام ارتفاع الطبقة ٠,١ مم، ودرجة حرارة الطباعة ٢٣٠ درجة مئوية، وسرعة الطباعة ٢٠ مم/ثانية تعطي أعلى قوة في العينات. ومع ذلك، فإن العينات المطبوعة بطبقة يبلغ ارتفاعها ٠,٢ مم، ودرجة حرارة الطباعة ٢٢٠ درجة مئوية، وسرعة الطباعة ٣٠ مم / ثانية تظهر أيضًا صلابة وقوة جيدة، وإن كانت أقل قليلاً من القيم

NJES is an **open access Journal** with **ISSN 2521-9154** and **eISSN 2521-9162**

القصوى. بالإضافة إلى ذلك، عند استخدام هذه الإعدادات المحددة (٠,٣ مم - ٢١٠ درجة مئوية - ٤٠ مم/ ثانية)، تقل الصفات الميكانيكية إلى الحد الأدنى.

1. Introduction

3D printing is a highly adaptable and groundbreaking technology that allows for the fabrication of complex and personalized objects with unparalleled accuracy [1, 2]. As the popularity of employing shape-memory polymers (SMPs) for basic science and biomedical applications grows, and as three-dimensional (3D) printing of SMPs grows simultaneously, it is essential to have exact control over the mechanical properties of a printed SMP component [3].

SMPs are increasingly attracting attention for several uses in 4D printing [4]. SMPs have the advantage of lower processing temperatures and costs compared to shape-memory alloys. Moreover, shape changing functionality in SMPs is better than in shape memory composites [4]. The smart materials like SMPs can change their shapes temporarily and then recover the original shapes after applying external stimuli on them [5]. Due to their unique thermo-mechanical properties, SMPs have attracted a lot of interest; therefore, these properties make them suitable for use in flexible electronics, aircraft components, medical instruments, etc. [6]. Nevertheless, the feasibility of using these types of materials in specific applications depends directly on the mechanical functionality of the printed structures [5].

Additive manufacturing, also called 3D printing, is a way of production that is done through the successive addition of fused material layers to build three-dimensional parts [7]. Fused deposition modeling (FDM) is a popular technique among additive manufacturing methods [4]. This method includes the 3D objects built by depositing the melted polymer across the nozzle onto the platform, where the computer-aided design data file specifies the way of construction, layers, and paths to build such items [4]. This method provides more efficient and cost-effective production of different items in comparison with conventional methods [8].

Generally, FDM procedures utilize thermoplastic polymers like acrylonitrile butadiene styrene (ABS), thermoplastic polyurethane (TPU), and polylactic acid (PLA) [9]. The mechanical properties of 3D printed SMPs are affected directly by the printing parameters used during the fabrication process, for example, printing temperature, printing speed, infill density, and layer thickness [10]. Therefore, it is important to regulate and match the factors of 3D printing with the resulting mechanical characteristics of the polymers to enhance practical applications [11]. Slight alterations in these parameters could have a significant impact on an object's properties, like elasticity, tensile strength, and shape memory characteristics [10]. For example, in the study of villacres et al., it was found that the printing angle and infill density resulted in various tensile stress, maximum, and strain elastic moduli of the polymer [12]. While Buj-corral investigated the effect of printing factors on the surface roughness, density, and dimensional accuracy of the SMP products [13]. In addition, the relationship between fiber inclination angle and shape recovery was investigated by Liu et al. [14]. Whereas Garcia Rosales et al. research was about examining the young's modulus, fixing ratio, and recovery ratio that were affected by changing layer thickness, printing temperature, and printing speed [15]. And the conclusion of this research was that the higher printing temperature, thicker layer thickness, and slower printing speeds produced a greater Young's modulus [15].

Our study seeks to investigate and describe the correlation between 3D printing parameters and the mechanical properties of the SMP. The results will provide a practical impression, which might lead to customizing the properties of SMP applications. To achieve this, the SMP thermoplastic polyurethane MM-3520 has been used. Cellular cubical specimens were printed by varying three printing factors: printing speed (20, 30, and 40 mm/s), printing temperature (210, 220, and 230 °C), and layer thickness (0.1, 0.2, and 0.3 mm). During the printing process, these parameters were adjusted and controlled carefully. During the printing process, these parameters were adjusted and controlled carefully. The compression test was performed to measure the influence of manufacturing factors on the mechanical properties.

2. Experimental

2.1. Material

In this research, we used a filament made of thermoplastic polyurethane pellets (MM-3520, SMP Technologies, Inc., Japan) to produce the cubical cellular specimens. This type of SMP is efficient enough to be used in FDM 3D printers [1].

2.2. Production

The samples were designed by CAD (SolidWorks, SolidWorks Corp., Dassault Systèmes, 2023) then they exported to UltiMaker Cura 5.4.0 software to specify printing parameters, slice and generate the required G-code of each sample. A desktop fused deposition modeling (FDM) 3D printer (ANYCUBIC MEGA Pro) with a nozzle size of 0.4 mm was employed to fabricate the specimens. The printing parameters are listed in Table 1.

Table (1): Fabrication parameters for 3D printing of scaffold test specimens.

Printing Parameters (Unit)	Values
Extrusion temperature (°C)	210, 220 and 230
Bed temperature (°C)	45
Nozzle diameter (mm)	0.4
Layer thickness (mm)	0.1, 0.2 and 0.3
Printing speed (mm/s)	20, 30 and 40
Infill pattern	Straight line

NJES is an **open access Journal** with **ISSN 2521-9154** and **eISSN 2521-9162**

Each set of samples included altering certain printing settings while keeping the others constant. As an example, when modifying the height of the printing layers (0.1, 0.2, and 0.3 mm), the printing speed and printing temperature remain constant at 30 mm/s and 220 °C respectively. Whereas the sets produced at different printing temperatures (210, 220, and 230 °C) maintained a constant printing speed of 30 mm/s and a layer thickness of 0.2 mm. This is also applied to the specimens of altered printing speed (20, 30, and 40 mm/s); they were printed with a 220 °C print temperature and a 0.1 mm layer height.

2.3. Microstructure analysis

The microstructures of the extruded filament and printed items were examined using an optical microscope (Olympus BX60M) at a magnification of x5.

2.4. Mechanical properties

The mechanical characteristics of the rectangular scaffold samples, measuring 16x16x16 mm as shown in Fig.1, were assessed using an Instron Universal testing machine (Testometric, M500-25kN). The force was exerted until the sample was compressed to around 50% of its initial length, using a cross-head speed of 1.3 mm/min. According to the specifications stated in ASTM standard D695-96, five scaffold samples were used in each group, all printed using identical settings. This was done to calculate an average value.

The design of scaffolds should typically mimic the porosity of bone tissue, which is around 70% [16, 17]. Although an ideal scaffold pore size for efficient bone regeneration has yet to be determined, studies have reported viable pore sizes ranging from 0.1 mm up to 1.2 mm [16]. The dimensions of the pores on the sides of the specimen, as seen in Fig.2, are 1 mm in height and 1.018 mm in width. On the other hand, the pores at the top and bottom of the specimen have dimensions of 1.018 mm in height and 1.018 mm in width. The scaffolds were fabricated for each condition using horizontal printing, which resulted in improved fiber alignment and bonding compared to other printing planes [18].

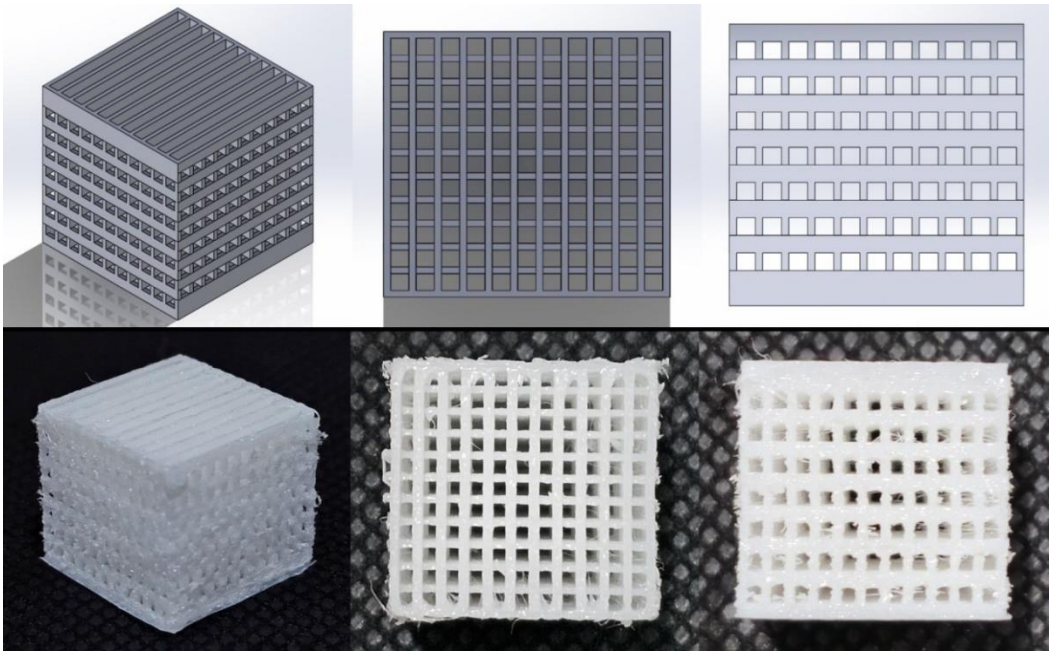

(a)

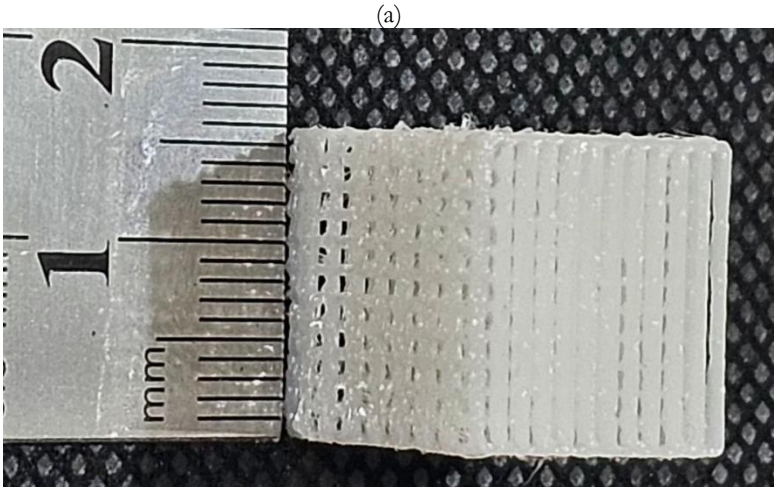

(b)

Figure (1): (a) Design of the sample from different views and (b) dimensions of the sample.

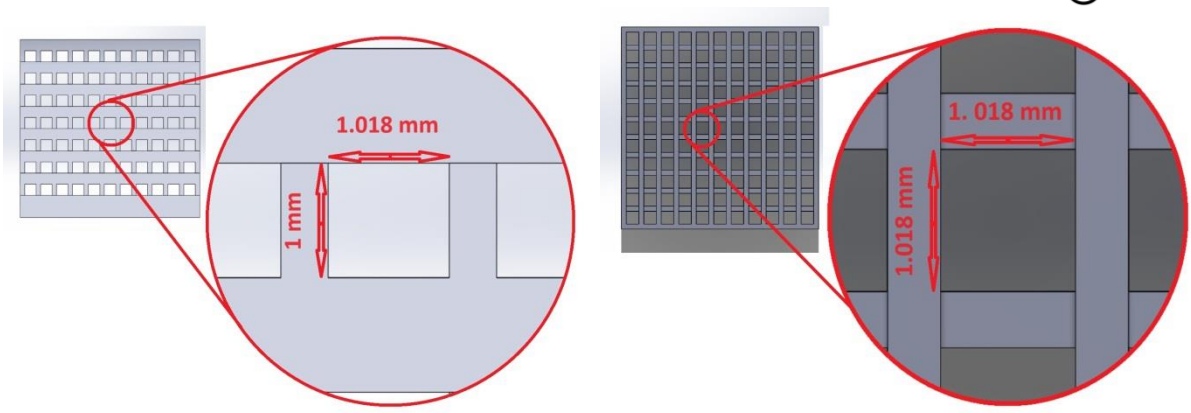

(a) (b)

Figure (2): (a) Dimensions of pores at the sides of specimen and (b) Dimensions of pores at the top and bottom of specimen.

2.5. Statistical analysis

The data were provided as the mean ± standard deviation. The statistical analysis was conducted using the one-way analysis of variances (ANOVA) in Origin Lab Pro 2024.

3. Results and discussion

3.1. Microstructure analysis

The layer height influences the microstructure of TPU-printed biomaterial. Thinner layers, such as 0.1 mm, exhibit over-compaction, the highest compression ratio to the extruded fibers during printing and the trace of the nozzle's movement appears more clearly on the printed layer[19]. This results in smoother surface finish. Increasing the layer height to 0.2 mm has reduced the compression ratio impact, decreasing the nozzle's trace and smoothness of the printed layer [20], as seen in the comparison between Fig.3 (a and b). The specimen with a layer thickness of 0.3 mm has lowest compaction ratio, therefore exhibiting a reduced connection area with a higher roughness in deposited fibers, seen in Fig.3 (c). Figure 4 (a, b, and c) illustrates the layer thickness impact at the joint areas of the structure. In the thinner layer thickness (0.1 mm) specimens, the printing is more accurate, and the connection between layers is better. While the thicker printed layers have lower quality and weaker bonds in the joint regions.

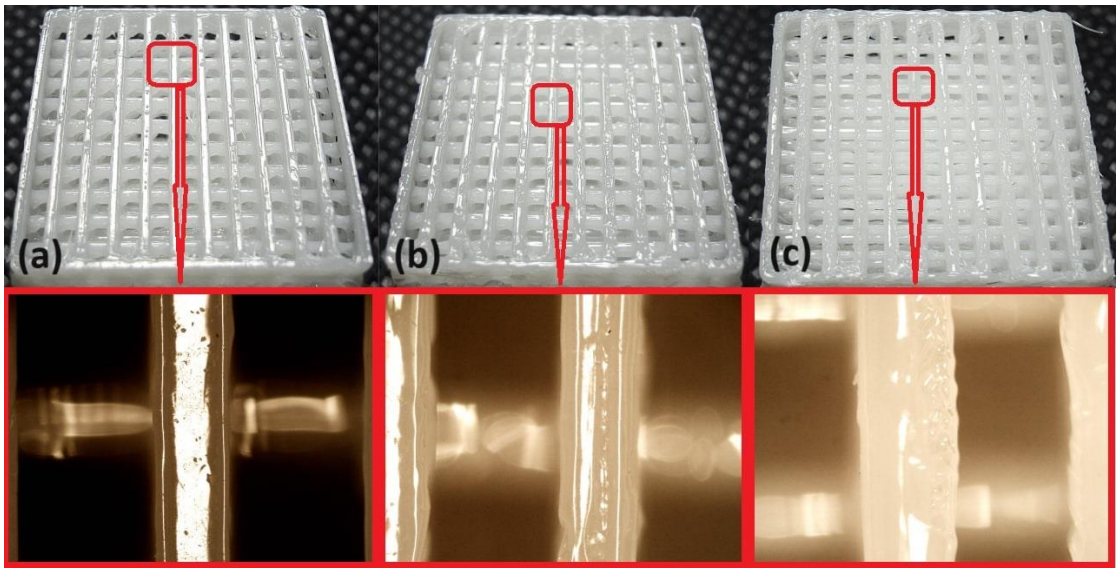

Figure (3): effect of layer thickness on the specimens' texture (a) 0.1 mm (b) 0.2 mm (c) 0.3 mm.

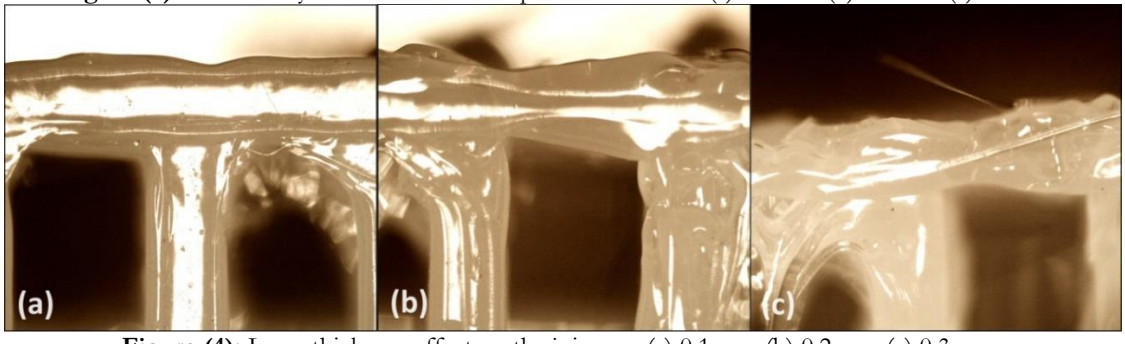

Figure (4): Layer thickness effect on the join area (a) 0.1 mm (b) 0.2 mm (c) 0.3 mm.

Figure 5 (a, b, and c) shows clearly the variation in the height of layer thickness from 0.1 mm to 0.3 mm. In addition, it illustrates that a thinner layer thickness results in a broader contact area, as indicated by the red lines. The wider contact area promotes the mechanisms of bonding and interdiffusion owing to an elevated compression ratio [19]. A layer height of 0.3 mm has the lowest compaction ratio, which leads to a narrow contact area found in the interlaminar zone, as seen in Fig.5 (c).

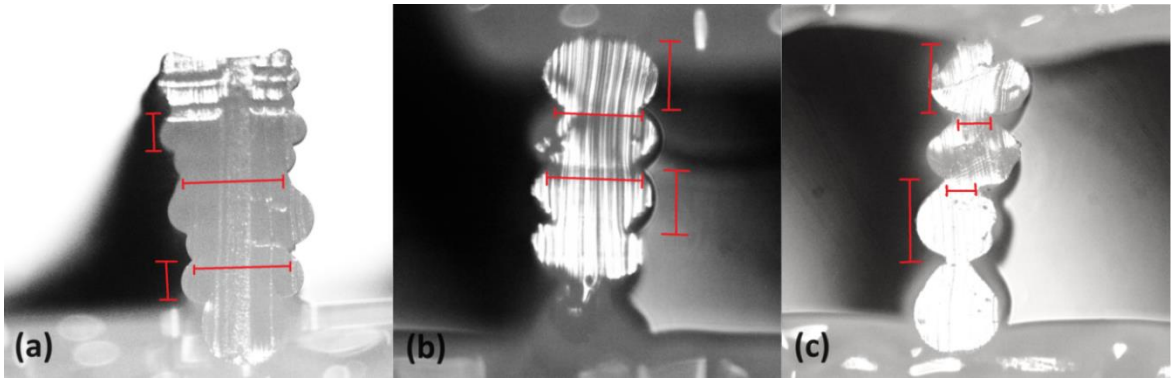

Figure (5): cross section view of contact area and porosities in (a) 0.1 mm (b) 0.2 mm (c) 0.3 mm specimens.

On the other hand, Raising the temperature enhances the polymer's flow and reduces its viscosity [21], resulting in smoother surfaces when comparing specimens printed at various temperatures (210, 220, and 230 °C) as seen in Fig.3 (b) and Fig.6 (a and b). Low temperature (210 °C in Fig.6 (a)) could affect the smooth extrusion of TPU filament through the nozzle. This would lead to irregular flow, blockages, flaws, and blemishes on the surface. Specimens printed at 220 °C revealed smoother surfaces and fewer flaws due to the increased flowability and reduced viscosity of the polymer at this temperature as seen at Fig.3 (b) [21]. The bubbles' presence in the samples at 230 °C will impact the surface quality findings. This flaw becomes apparent at high temperatures as the material becomes almost liquid as it enters the extruder nozzle, but it is essentially non-existent at lower temperatures. Other authors suggest that greater temperatures lead to a reduction in viscosity. As the polymer moves across the nozzle, produces friction with the walls which in turn generates turbulence contributing to the air intake [20-22]. Figures 4 (b) and 7 (a and b) illustrate the printing temperature impact at the joint areas of the structure. In the specimens with the highest printing temperature (230 °C), the polymer would be more viscous and flowable [23]; therefore, more material would be extruded from the nozzle, which results in a wider connection area. Lower printing temperatures (210 °C and 220 °C) would produce lower printing quality and thinner bonds in the regions of joints from the previous temperature (230 °C). The comparison of the cross-sectional views in Fig.5 (b) and 8 show that at various temperatures, the polymer becomes almost liquid before reaching the extruder nozzle [23], causing the width of the extruded filament to expand. Consequently, the contact area between the two stacked fibers also increases. A rise in extruder temperature leads to a higher part density due to a drop in the viscosity of the SMP material, allowing it to flow more smoothly through the nozzle [23]. This results in an increased amount of material being used to create the model [23].

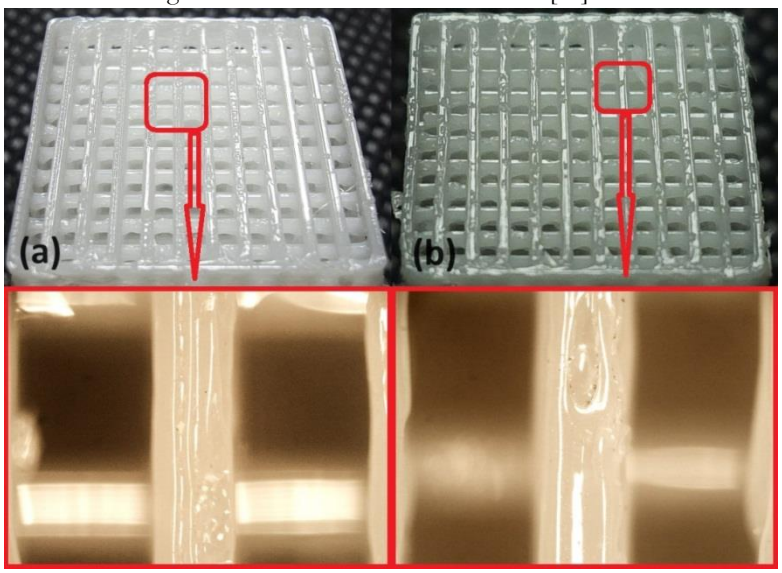

Figure (6): Illustration the top view texture of the printed specimens with (a) 210 °C (b) 230 °C.

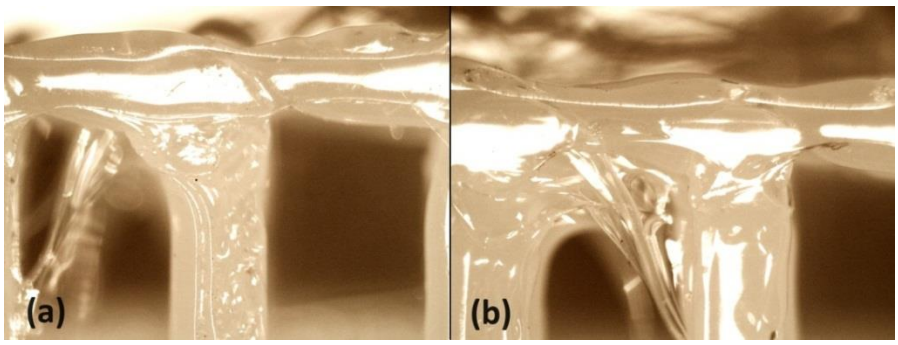

Figure (7): Printing temperature effect on the join area (a) 210 °C (b) 230 °C.

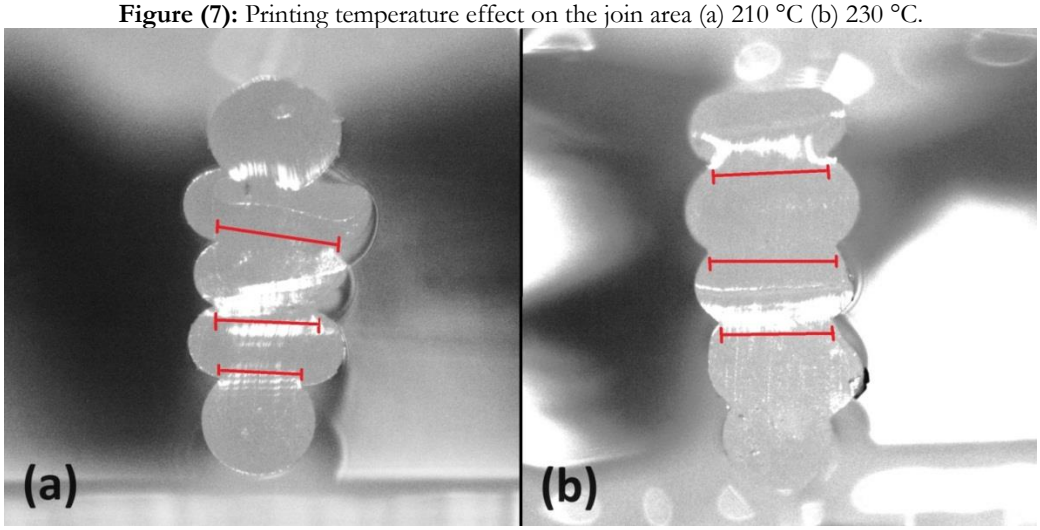

Figure (8): Cross-section view of specimen printed with (a) 210 °C and (a) 230 °C.

Our investigation verified that the printing speed impacts the deposition of filaments, thus influencing print quality. Irregularities arose in the curved sections, breadth, and connections of stacked filaments because of the inadequate coordination between the printing speed and extrusion speed. The image analysis findings indicated that the deposition of SMP filaments was successful at printing rates of 20, 30, and 40 mm/s, as shown in Fig.3 (b) and Fig.9 (a and b). At increased velocities, the extruded filaments experienced a deformed and rough surface. The breadth of the filaments within a layer was inconsistent and variable, as seen in Fig.9 (b). Higher printing rates caused issues with filament feeding into the extrusion nozzle owing to the filament's lack of stiffness, leading to interruptions in the extrusion process [22]. When the printing speeds get slower (20 mm/s and 30 mm/s), they produced smooth layer and better surface finish. Additionally, Figures 4 (b) and 10 (a and b) show the printing speed effect at the joint areas of the structure. In the specimens with the higher printing speeds, the amount of polymer extrusion would not be proportionate with the speed of nozzle movement [23]; therefore, inadequate material would be extruded from the nozzle, which results in a weaker connection area [20]. Lower printing speed (20 mm/s) would produce higher printing quality and wider bonds in the regions of joints when compared to the previous speeds (30 and 40 mm/s).

Another discovery has been made that temperature and holding time significantly impact bond formation [24]. Additionally, the cavities occur within the red circle in Fig.11 when TPU infill filaments elongate at higher printing speeds [20]. It is shown that the density of the specimen reduces as the scanning speed of the nozzle increases. Insufficient material extrusion due to high scanning speed would lead to the formation of voids and cavities [22], as seen in Fig.11.

3.2. Mechanical properties

In addition to promoting bone tissue development by filling bone deficiencies, the scaffolds must also possess sufficient structural integrity to resist the forces exerted during regular walking. The ground exerts a response force on the foot when walking that is 1.5 times the individual's body weight. The femur has a diameter ranging from 6 to 10 cm. Typically, the narrowest part of the femur for an adult weighing 60 Kg is around 6 cm. Thus, when a scaffold is placed in this location, it will endure a stress of 0.21 MPa. The scaffolds will satisfy the mechanical criterion if the yield strength exceeds 0.252 MPa, assuming a safety factor of 1.2 [25]. In order to examine the compressive characteristics, compression tests were carried out at room temperature using the settings specified in section (2.3). Figure 12 shows the specimen before and after compression test.

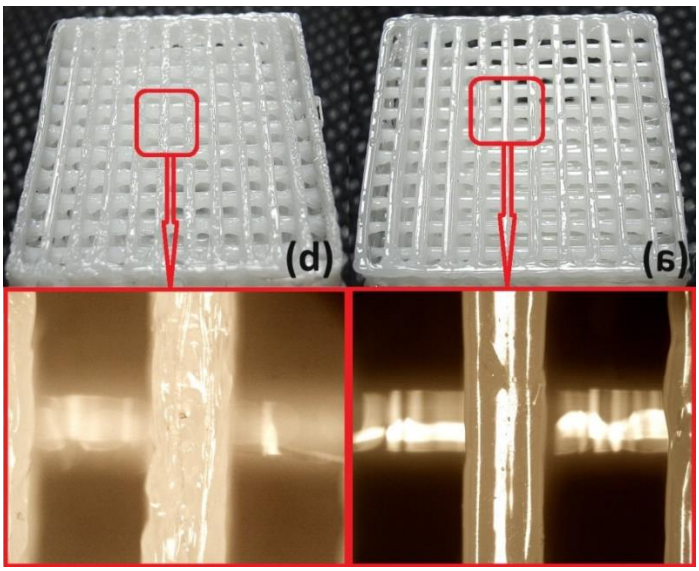

Figure (9): Top view texture of specimens printed with (a) 20 mm/s and (b) 40 mm/s.

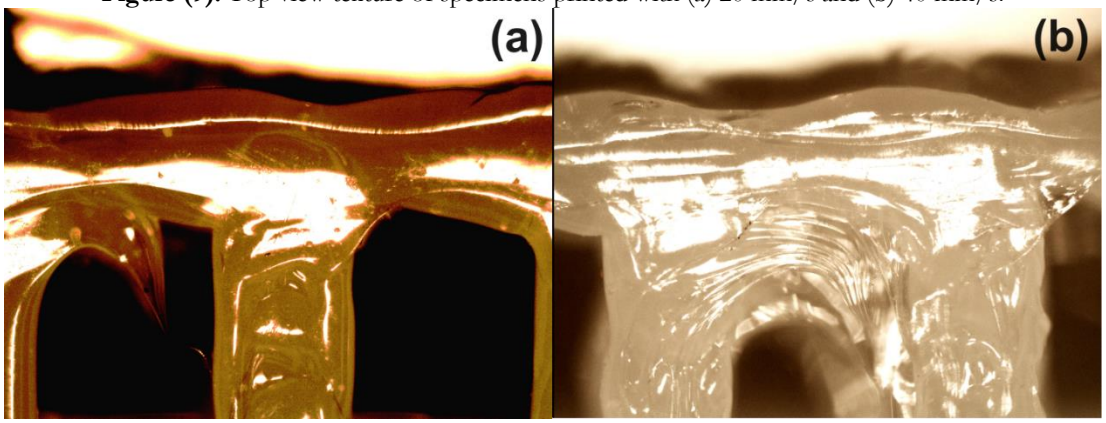

Figure (10): Printing temperature effect on the join area (a) 20 mm/s and (b) 40 mm/s.

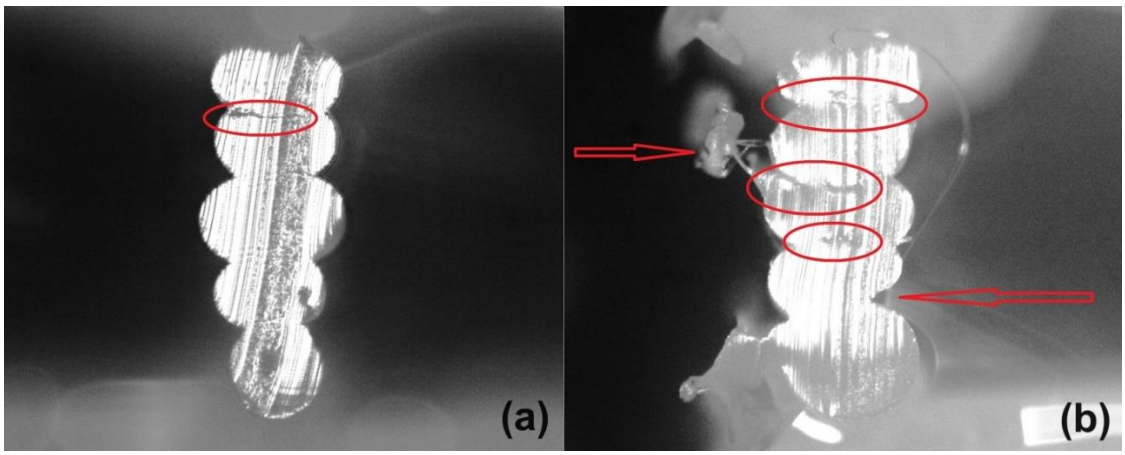

Figure (11): Cross-sectional view of specimens printed with (a) 20 mm/s and (b) 40 mm/s.

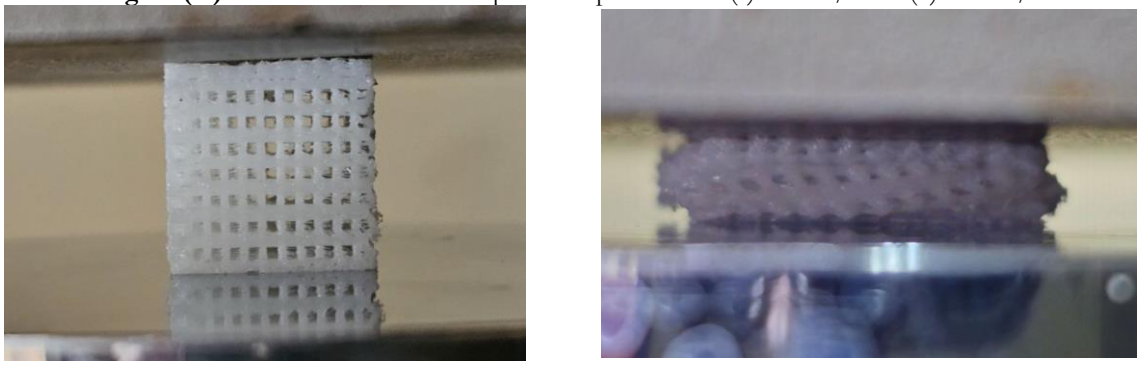

(a) (b)

Figure (12): (a) specimen before compression and (b) specimen after compression.

The mechanical compressive strength of the reference face-centered cubic topology specimens, printed with various parameters, is illustrated in Figures 13, 14, and 15. By analyzing the stress-strain curve of the mechanical response, The phase of deformation is triggered by the destabilization and the onset of bending and buckling mechanisms within one of the structural layers (which encompasses the average peak stress (σ_p), defined as the stress at which the cells in the polymer structure commence collapsing under compression) [26-28]. An analysis of variances (ANOVAs) was performed to evaluate the values of σ_p for various printing parameter settings.

Figure 13 shows the peak stress (σ_p) of the three scaffolds as the layer thickness varies (0.1, 0.2, and 0.3 mm) while keeping other parameters such as printing temperature (220 °C) and printing speed (30 mm/s) constant. The samples generated with layer thicknesses of 0.1, 0.2, and 0.3mm exhibit peak stresses of 0.5554±0.08498, 0.5213±0.069, and 0.3975±0.041 MPa respectively. Decreasing the thickness of the layers in 3D printed TPU (Thermoplastic Polyurethane) would greatly improve σ_p of the final product. By reducing the layer height from 0.3 mm to 0.1 mm, the adhesion between each layer and the one below it improves, resulting in enhanced interlayer bonding. The enhanced adhesion reduces the risk of separation and improves the overall strength of the printed item. In addition, thinner layers result in a more polished surface, fewer voids, and increased sample density. In turn, this reduces the risk of stress concentration spots that might potentially undermine the compressive strength [29-31]. Also the findings in section 3.1 demonstrate that the compression ratio, reflecting the pressure on the filament during printing, may enhance the mechanical and microstructural characteristics by affecting the bonding process between the printed layers [21].

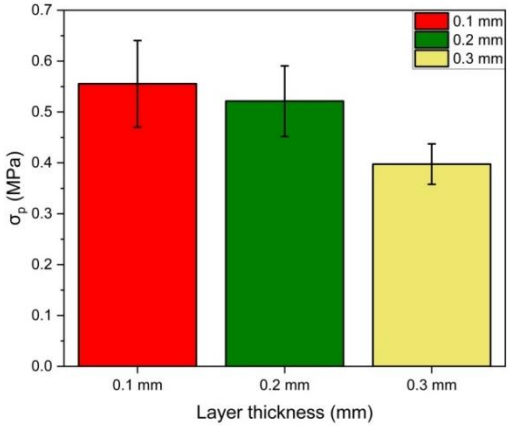

Figure (13): Peak stress of samples printed with (0.1, 0.2 and 0.3 mm) layer thickness.

Increasing the printing temperature from 210 to 230 °C for 3D-printed TPU would enhance its compressive strength as seen in Fig.14. TPU is a thermoplastic polymer that experiences changes in its physical state throughout the printing process. Raising the temperature improves the polymer's ability to flow and decreases its viscosity, resulting in increased contact area, improved interlayer adhesion, and the alignment of molecules. The enhanced adhesion between layers leads to a stronger and more unified structure, thereby raising the elastic stiffness and peak stress of the product [31, 33, 34]. In addition, Lower heating temperatures cause incomplete melting of crystalline areas, whereas higher printing temperatures provide more energy and allow for extra heating time for SMP TPU MM-3520 to crystallize. Therefore, the increased temperature enhances the crystallinity, thereby improving the mechanical characteristics of the product [20]. Finally, a higher printing temperature may result in elevated peak stress (σ_p), due to the material's enhanced resistance to deformation [29, 31].

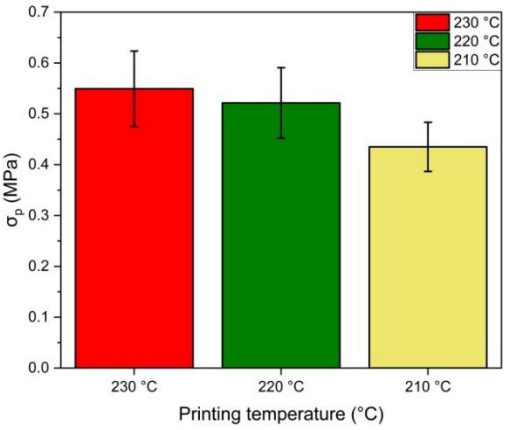

Figure (14): Peak stress of samples printed with (210, 220 and 230 °C) printing temperature.

Lowering the printing velocity from 40 to 20 mm/s during the 3D printing process of TPU could significantly improve the linear peak stress as shown in Fig.15. Reduced printing rates provide improved heat dissipation and enhanced layer adhesion. Reducing the speed of the printing process allows each layer to have a longer duration for bonding with the previous layer, resulting in the formation of stronger connections between layers as illustrated in previous section (3.1). The improved bonding is essential for strengthening the entire structure of the 3D-printed TPU item, especially in situations where compressive strength is of utmost importance [30, 31, 35, 36].

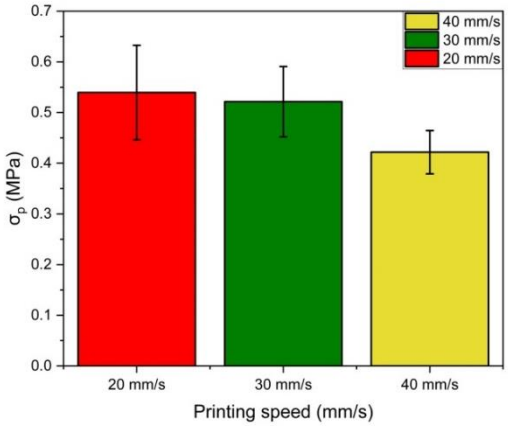

Figure (15): Peak stress of samples printed with (20, 30 and 40 mm/s) printing speed.

Furthermore, higher printing rates lead to decreased mechanical characteristics because of the shorter forming period, which reduces the crystallinity of TPU. Each successive layer will be placed on the preceding layer during printing and will solidify the

liquid TPU. Insufficient contact time between layers and infill filaments reduces the time for polymer chains to disperse and crystallize, resulting in better bonding of the polymer infill filaments [20].

By adjusting the printing speed of this polymer, one may expect changes in peak stress (σ_p) amount. Reducing the printing speed may enhance the bonding between layers and promote a more orderly arrangement of molecules. The reason for this is that a reduced printing speed facilitates enhanced interlayer adhesion and provides an additional opportunity for the polymer to undergo cooling and solidification [29, 31].

4. Conclusion

The findings of this research indicate that the printing factors, including layer thickness, printing temperature, and printing speed, have a substantial impact on the compressive strength of 3D-printed TPU. The strength of the 3D printed item generally increase as the layer thickness and printing speed decrease as well as the printing temperature increases. Modifying these parameters resulted in comparable peak stress, exhibiting varied magnitudes irrespective of the infill design or infill percentage. While the samples produced at a speed of 20 mm/s, with a layer thickness of 0.1 mm, and at a temperature of 230 °C exhibit increased strength under compression, these parameters may not be regarded as optimal. Still, when looking at the stress-strain curve, you should also think about things like the material's elastic stiffness, plateau stiffness, and densification, as these directly affect how stress is distributed and how much energy is absorbed when the load is applied. Consequently, these properties enable us to choose the right parameters that should be used for the future improvement of 3D-printed scaffolds in specific applications. Moreover, the producers and 3D printing enthusiasts have access to a wide range of infill patterns and settings via different slicing tools. This research examined a limited number of factors for the same specimen design, which may not include the most suitable features for certain applications. These findings provide a valuable foundation for future exploration into the impact of various printing settings on the performance of 3D-printed bone scaffold designs.

5. Reference:

[1] Pieri, K., et al., Printing Parameters of Fused Filament Fabrication Affect Key Properties of Four-Dimensional Printed Shape-Memory Polymers. 3D Printing and Additive Manufacturing, 2023. **10**(2): p. 279-288, https://doi.org/10.1089/3dp.2021.0072.

[2] Kafle, A., et al., 3D/4D Printing of polymers: Fused deposition modelling (FDM), selective laser sintering (SLS), and stereolithography (SLA). Polymers, 2021. **13**(18): p. 3101, https://doi.org/10.3390/polym13183101.

[3] Sheoran, A.J. and H. Kumar, Fused Deposition modeling process parameters optimization and effect on mechanical properties and part quality: Review and reflection on present research. Materials Today: Proceedings, 2020. **21**: p. 1659-1672, https://doi.org/10.1016/j.matpr.2019.11.296.

[4] Valvez, S., et al., Fused filament fabrication-4d-printed shape memory polymers: A review, Polymers (Basel) 13 (2021) 1–25, https://doi.org/10.3390/polym13050701.

[5] Zhao, W., et al., Research progress of shape memory polymer and 4D printing in biomedical application. Advanced Healthcare Materials, 2023. **12**(16): p. 2201975, https://doi.org/10.1002/adhm.202201975.

[6] Cavender-Word, T.J. and D.A. Roberson, Development of a Resilience Parameter for 3D-Printable Shape Memory Polymer Blends. Materials, 2023. **16**(17): p. 5906, https://doi.org/10.3390/ma16175906.

[7] Mehrpouya, M., et al., 4D printing of shape memory polylactic acid (PLA). Polymer, 2021. **230**: p. 124080, https://doi.org/10.1016/j.polymer.2021.124080.

[8] García-Dominguez, A., J. Claver, and M.A. Sebastián, Integration of additive manufacturing, parametric design, and optimization of parts obtained by fused deposition modeling (FDM). A methodological approach. Polymers, 2020. **12**(9): p. 1993, https://doi.org/10.3390/polym12091993.

[9] Ehrmann, G. and A. Ehrmann. Shape-memory properties of 3D printed PLA structures. in Proceedings. 2020. MDPI, https://doi.org/10.3390/CGPM2020-07198.

[10] Ambati, S.S. and R. Ambatipudi, Effect of infill density and infill pattern on the mechanical properties of 3D printed PLA parts. Materials Today: Proceedings, 2022. **64**: p. 804-807, https://doi.org/10.1016/j.matpr.2022.05.312.

[11] Wickramasinghe, S., T. Do, and P. Tran, FDM-based 3D printing of polymer and associated composite: A review on mechanical properties, defects and treatments. Polymers, 2020. **12**(7): p. 1529, https://doi.org/10.3390/polym12071529.

[12] Villacres, J., D. Nobes, and C. Ayranci, Additive manufacturing of shape memory polymers: effects of print orientation and infill percentage on shape memory recovery properties. Rapid Prototyping Journal, 2020. **26**(9): p. 1593-1602, https://doi.org/10.1108/RPJ-09-2019-0239.

[13] Buj-Corral, I., A. Bagheri, and M. Sivatte-Adroer, Effect of printing parameters on dimensional error, surface roughness and porosity of FFF printed parts with grid structure. Polymers, 2021. **13**(8): p. 1213, https://doi.org/10.3390/polym13081213.

[14] Liu, T., et al., 4D printed anisotropic structures with tailored mechanical behaviors and shape memory effects. Composites Science and Technology, 2020. **186**: p. 107935, https://doi.org/10.1016/j.compscitech.2019.107935.

[15] Rosales, C.A.G., et al., Characterization of shape memory polymer parts fabricated using material extrusion 3D printing technique. Rapid

Prototyping Journal, 2018. **25**(2): p. 322-331, https://doi.org/10.1108/RPJ-08-2017-0157.

[16] Contreras Raggio, J.I., et al., Height-to-Diameter Ratio and Porosity Strongly Influence Bulk Compressive Mechanical Properties of 3D-Printed Polymer Scaffolds. Polymers, 2022. **14**(22): p. 5017, https://doi.org/10.3390/polym14225017.

[17] Abdal-hay, A., et al., A review of protein adsorption and bioactivity characteristics of poly ε-caprolactone scaffolds in regenerative medicine. European Polymer Journal, 2022. **162**: p. 110892, https://doi.org/10.1016/j.eurpolymj.2021.110892.

[18] Liu, H., et al., Three-dimensional printing of poly (lactic acid) bio-based composites with sugarcane bagasse fiber: Effect of printing orientation on tensile performance. Polymers for Advanced Technologies, 2019. **30**(4): p. 910-922, https://doi.org/10.1002/pat.4524.

[19] Ursini, C. and L. Collini, Fdm layering deposition effects on mechanical response of tpu lattice structures. Materials, 2021. **14**(19): p. 5645, https://doi.org/10.3390/ma14195645.

[20] Le, D., et al., Optimizing 3D printing process parameters for the tensile strength of thermoplastic polyurethane plastic. Journal of Materials Engineering and Performance, 2023: p. 1-12, https://doi.org/10.1007/s11665-023-07892-8.

[21] Vidakis, N., et al., Strain rate sensitivity of polycarbonate and thermoplastic polyurethane for various 3d printing temperatures and layer heights. Polymers, 2021. **13**(16): p. 2752, https://doi.org/10.3390/polym13162752.

[22] Wang, P., B. Zou, and S. Ding, Modeling of surface roughness based on heat transfer considering diffusion among deposition filaments for FDM 3D printing heat-resistant resin. Applied Thermal Engineering, 2019. **161**: p. 114064, https://doi.org/10.1016/j.applthermaleng.2019.114064.

[23] Pivar, M., D. Gregor-Svetec, and D. Muck, Effect of printing process parameters on the shape transformation capability of 3D printed structures. Polymers, 2021. **14**(1): p. 117, https://doi.org/10.3390/polym14010117.

[24] Peng, W., et al., Effects of FDM-3D printing parameters on mechanical properties and microstructure of CF/PEEK and GF/PEEK. Chinese Journal of Aeronautics, 2021. **34**(9): p. 236-246, https://doi.org/10.1016/j.cja.2020.05.040.

[25] Zhao, W., et al., Porous bone tissue scaffold concept based on shape memory PLA/Fe3O4. Composites Science and Technology, 2021. **203**: p. 108563, https://doi.org/10.1016/j.compscitech.2020.108563.

[26] Nace, S.E., et al., A comparative analysis of the compression characteristics of a thermoplastic polyurethane 3D printed in four infill patterns for comfort applications. Rapid Prototyping Journal, 2021. **27**(11): p. 24-36, https://doi.org/10.1108/RPJ-07-2020-0155.

[27] Platek, P., et al., Deformation process of 3D printed structures made from flexible material with different values of relative density. Polymers, 2020. **12**(9): p. 2120, https://doi.org/10.3390/polym12092120.

[28] Zhang, C., et al., Compression Behavior of 3D Printed Polymer TPU Cubic Lattice Structure. Materials Research, 2022. **25**, https://doi.org/10.1590/1980-5373-MR-2022-0060.

[29] Pazhamannil, R.V., et al., Investigations into the effect of thermal annealing on fused filament fabrication process. Advances in Materials and Processing Technologies, 2022. **8**(sup2): p. 710-723, https://doi.org/10.1080/2374068X.2021.1946753.

[30] Dave, H.K. and J.P. Davim, Fused deposition modeling based 3D printing. 2021: Springer, https://doi.org/10.1007/978-3-030-68024-4.

[31] Ameen, A.A., A.M. Takhakh, and A. Abdal-hay, An Overview of the Latest Research on the Impact of 3D Printing Parameters on Shape Memory Polymers. European Polymer Journal, 2023: p. 112145, https://doi.org/10.1016/j.eurpolymj.2023.112145.

[32] Farkas, A.Z., S.-V. Galatanu, and R. Nagib, The Influence of Printing Layer Thickness and Orientation on the Mechanical Properties of DLP 3D-Printed Dental Resin. Polymers, 2023. **15**(5): p. 1113, https://doi.org/10.3390/polym15051113.

[33] Zeng, C., et al., 4D printed electro-induced continuous carbon fiber reinforced shape memory polymer composites with excellent bending resistance. Composites Part B: Engineering, 2020. **194**: p. 108034, https://doi.org/10.1016/j.compositesb.2020.108034.

[34] Abdal-hay, A., et al., Fabrication of biocompatible and bioabsorbable polycaprolactone/magnesium hydroxide 3D printed scaffolds: Degradation and in vitro osteoblasts interactions. Composites Part B: Engineering, 2020. **197**: p. 108158, https://doi.org/10.1016/j.compositesb.2020.108158.

[35] Sharma, R., R. Singh, and A. Batish, On mechanical and surface properties of electro-active polymer matrix-based 3D printed functionally graded prototypes. Journal of Thermoplastic Composite Materials, 2022. **35**(5): p. 615-630, https://doi.org/10.1177/0892705720907677.

[36] Bartnikowski, M., et al., A comprehensive study of acid and base treatment of 3D printed poly (ε-caprolactone) scaffolds to tailor surface characteristics. Applied Surface Science, 2021. **555**: p. 149602, https://doi.org/10.1016/j.apsusc.2021.149602.